Physics in Medicine & Biology

PAPER

Acoustic cavitation-based monitoring of the reversibility and permeability of ultrasound-induced blood-brain barrier opening

To cite this article: Tao Sun *et al* 2015 *Phys. Med. Biol.* **60** 9079

IOP Publishing | Institute of Physics and Engineering in Medicine Physics in Medicine & Biology

Phys. Med. Biol. **60** (2015) 9079–9094 doi:10.1088/0031-9155/60/23/9079

Acoustic cavitation-based monitoring of the reversibility and permeability of ultrasound-induced blood-brain barrier opening

Tao Sun[1,3], Gesthimani Samiotaki[1], Shutao Wang[1], Camilo Acosta[1], Cherry C Chen[1] and Elisa E Konofagou[1,2]

[1] Department of Biomedical Engineering, Columbia University, New York, NY, USA
[2] Department of Radiology, Columbia University, New York, NY, USA

E-mail: ek2191@columbia.edu

Received 16 July 2015, revised 11 September 2015
Accepted for publication 6 October 2015
Published 12 November 2015

Abstract

Cavitation events seeded by microbubbles have been previously reported to be associated with MR- or fluorescent-contrast enhancement after focused ultrasound (FUS)-induced blood-brain barrier (BBB) opening. However, it is still unknown whether bubble activity can be correlated with the reversibility (the duration of opening and the likelihood of safe reinstatement) and the permeability of opened BBB, which is critical for the clinical translation of using passive cavitation detection to monitor, predict and control the opening. In this study, the dependence of acoustic cavitation on the BBB opening duration, permeability coefficient and histological damage occurrence were thus investigated. Transcranial pulsed FUS at 1.5 MHz in the presence of systemically circulating microbubbles was applied in the mouse hippocampi ($n = 60$). The stable and inertial cavitation activities were monitored during sonication. Contrast-enhanced MRI was performed immediately after sonication and every 24 h up to 6 d thereafter, to assess BBB opening, brain tissue permeability and potential edema. Histological evaluations were used to assess the occurrence of neurovascular damages. It was found that stable cavitation was well correlated with: (1) the duration of the BBB opening ($r^2 = 0.77$); (2) the permeability of the opened BBB ($r^2 = 0.82$); (3) the likelihood of safe opening ($P < 0.05$, safe opening compared to cases of damage; $P < 0.0001$, no opening compared to safe opening). The inertial cavitation dose was correlated with the resulting BBB permeability ($r^2 = 0.72$). Stable cavitation was found

[3] Current Address: Focused Ultrasound Laboratory, Brigham and Women's Hospital, Harvard Medical School, 221 Longwood Avenue, Boston, MA 02115. E-mail: taosun@bwh.harvard.edu

to be more reliable than inertial cavitation at assessing the BBB opening within the pressure range used in this study. This study demonstrates that the stable cavitation response during BBB opening holds promise for predicting and controlling the restoration and pharmacokinetics of FUS-opened BBB. The stable cavitation response therefore showed great promise in predicting the BBB opening duration, enabling thus control of opening according to the drug circulation time. In addition, avoiding adverse effects in the brain and assessing the pharmacokinetics of the compounds delivered can also be achieved by monitoring and controlling the stable cavitation emissions.

Keywords: acoustic cavitation, treatment monitoring, blood-brain barrier, drug delivery, passive cavitation detection, microbubble, focused ultrasound

(Some figures may appear in colour only in the online journal)

1. Introduction

Focused ultrasound (FUS) with systemically administered microbubbles has been shown to transiently induce localized and reversible blood-brain barrier (BBB) opening for drug delivery to the brain (Hynynen and McDannold 2001, Burgess and Hynynen 2013). BBB prevents permeation of molecules greater than 400 Da from the vasculature to the brain parenchyma, rendering many potent drugs ineffective (Pardridge 2005). Induced by FUS, oscillating microbubbles enhance local mechanical effects to the targeted vasculature, facilitating the transient opening of the BBB in the regions of interest (Aryal *et al* 2014) and the improvements of other brain drug delivery paradigms (Chen *et al* 2014, Wang *et al* 2014b). Several therapeutic agents have thus been successfully delivered including antibodies (Kinoshita *et al* 2006, Raymond *et al* 2008), chemotherapeutic agents (Liu *et al* 2010, Park *et al* 2012, Treat *et al* 2012), viral vectors (Thévenot *et al* 2012, Hsu *et al* 2013, Wang *et al* 2015), and neurotrophic factors (Wang *et al* 2012, Samiotaki *et al* 2015).

One key element to be established prior to clinical translation is to develop a real-time feedback indicator to control and predict the physiological changes after BBB opening. Contrast-enhanced MRI has been employed to detect the opening (Hynynen and McDannold 2001, Tung *et al* 2011a, McDannold *et al* 2012), assess any potential damage (Tung *et al* 2011b, McDannold *et al* 2012), map the permeability (Vlachos *et al* 2010, Park *et al* 2012) and monitor BBB closing (Samiotaki *et al* 2012). However, MRI-based evaluation of these physiological parameters, especially the reversibility and permeability, cannot be implemented with high temporal efficiency.

On the other hand, it has been well accepted that the microbubble cavitation activity plays a critical role in FUS-induced BBB opening (Tung *et al* 2011b). Stable volumetric microbubble oscillation (stable cavitation) and/or transient bubble collapse (inertial cavitation) due to associated oscillations have been previously investigated (McDannold *et al* 2006, Tung *et al* 2010, 2011a, 2011b, O'Reilly and Hynynen 2012). Transcranial passive cavitation detection (PCD) serves as a powerful tool in detecting microbubble activity in real time by characterizing their strength, mode and location through the scattering signature (Arvanitis *et al* 2013).

The feasibility of correlating acoustic cavitation emissions with BBB opening assessments has previously been reported (McDannold *et al* 2006, Tung *et al* 2011b, Arvanitis *et al* 2012, O'Reilly and Hynynen 2012, Fan *et al* 2014). Harmonic (Arvanitis *et al* 2012) and ultraharmonic (O'Reilly and Hynynen 2012) emissions have been proposed as indicator candidates of opening outcomes. However, most of the previous studies used MRI contrast techniques (Tung *et al* 2011b, Arvanitis *et al* 2012, O'Reilly and Hynynen 2012) to assess the opening

volume. The reversibility and permeability of the opened BBB may be more vital in clinical applications. The reversibility was depicted by the duration of BBB opening and the likelihood of safe opening. Predicting and controlling the reversibility (the duration of opening and the likelihood of safe reinstatement) are important because (1) the duration of the BBB opening is critical for drug delivery because different drugs have distinct circulation times; (2) developing a real-time indicator to assess the likelihood of safe opening during FUS exposure is vital for to minimize collateral damage. The permeability coefficient K_{trans} represents the pharmacokinetics of the MR tracer through the opened BBB, and it was shown to be associated with BBB opening volume and closing timelines (Vlachos *et al* 2011, Samiotaki *et al* 2012). This coefficient was also found to be correlated with the payload of a chemotherapy agent (doxorubixin) (Park *et al* 2012), indicating that the K_{trans} has the potential to indicate drug delivery to the brain after BBB opening.

In the current study, we investigate the role of acoustic cavitation in the restoration and pharmacokinetics of FUS-opened BBB, aiming at evaluating the cavitation monitoring in its assessments of the permeability, duration, and safety of BBB opening. Microbubble activity in response to ultrasound are dependent upon their initial dimensions and acoustic pressures (Ferrara *et al* 2007, Qin *et al* 2009, Tung *et al* 2011b). Here, monodisperse microbubbles with three different diameter ranges (1–2, 4–5, and 6–8 μm) in acoustic fields at different pressure amplitudes were thus used to induce variant cavitation activities. Cavitation activity was monitored during FUS treatment and quantitatively correlated with the time for BBB to close, the permeability coefficient and the histological damage occurrence.

2. Materials and methods

2.1. Animals

All animal studies presented herein were approved by the Columbia University Institutional Animal Care and Use Committee. A total of 60 male mice (Weight: 24.21 $\pm$ 1.72 g; C57BL/6, Harlan Laboratories, Indianapolis, IN) were anesthetized with a mixture of oxygen (0.8 L min^{-1} at 1.0 bar, 21 °C) and 1.5–2.0% vaporized isoflurane (SurgiVet, Smiths Medical PM, Dublin, OH) during treatment. The fur on the scalp was removed by an electric trimmer and depilatory cream in order to minimize acoustic impedance mismatch.

2.2. Microbubble preparation

Lipid-shelled monodisperse microbubbles with three different diameter ranges (1–2, 4–5, and 6–8 μm) were prepared in-house and size-isolated using the differential centrifugation method according to a previously published protocol (Feshitan *et al* 2009). A Multisizer III particle counter (Beckman Coulter, Opa Locka, FL) with a 30 μm aperture was used to measure the size distribution and concentration. The concentration of microbubble solution was diluted using phosphate-buffered saline (PBS) to 8×10^8 numbers ml^{-1} prior to intravenous administration through the tail vein.

2.3. FUS

A single-element, spherical-segment FUS transducer (center frequency: 1.5 MHz; focal length: 60 mm, diameter: 60 mm; Imasonic SAS, Voray-sur-l'Ognon, France) was driven by a function generator (33220A, Agilent, Palo Alto, CA). A 50 dB power amplifier (325LA, Electronic Navigation Industries, Rochester, NY) was used to amplify the transmitted waves.

Microbubbles in the systematic circulation interacted with the transmitted ultrasound, and the re-radiated waves from microbubbles were received by a single-element FUS transducer (center frequency: 10 MHz; focal length: 60 mm; diameter: 22.4 mm; Olympus NDT, Waltham, MA). This cavitation detector was positioned through a central hole of the FUS transducer so that their foci overlapped. Cavitation signal acquisition was controlled by a pulser-receiver system (Olympus NDT, Waltham, MA) that was connected to a digitizer (Gage Applied Technologies Inc., Lachine, QC, Canada).

A 5 s sonication with a pulse repetition frequency (PRF) of 5 Hz and pulse length (PL) of 100 cycles was carried out prior to microbubble administration in order to obtain an acoustic response baseline, which was used to normalize the cavitation dose quantification. Upon completion of the microbubble injection, 60 s FUS with the same PRF and PL was applied to the targeted area. The peak rarefactional pressures (PRPs) *in situ* were estimated according to the calibration described in our previous reports (Wang *et al* 2014a). The right hippocampus was targeted following a grid-guided targeting procedure (Choi *et al* 2007) while the left served as the control. The FUS focus was placed 3 mm beneath the skull so that the focal region overlapped with the hippocampus (Tung *et al* 2011b).

2.4. Cavitation signal acquisition and analysis

The cavitation dose was calculated based on the integrated area under the curve of temporal power variance of the cavitation signals monitored during FUS exposure. Two cavitation parameters that characterize the cavitation behaviors were calculated: stable cavitation dose (SCD) and inertial cavitation dose (ICD). The SCD was an indicator of the strength of stable oscillation. Each PCD-recorded pulse was transformed into a power spectrum using a fast Fourier transform at a sampling frequency of 50 MHz. Harmonic and ultraharmonic components were identified as the peak value within a 300 kHz bandwidth around each harmonic (nf_c, $n = 1, 2, 3\ldots$ $f_c = 1.5$ MHz) and a 100 kHz bandwidth around each ultraharmonic ($nf_c/2$, $n = 3, 5, 7\ldots$) frequency in the range between 4 and 12 MHz. The SCD was then quantified by integrating the amplitude of the harmonic and ultraharmonic responses over the entire sonication duration. The ICD, which represented the scale of microbubble collapsing, was quantified based on the root mean square (RMS) of the broadband emission amplitude within specific in-harmonic windows (bandwidth: 400 kHz) between 4 and 12 MHz. These RMS amplitudes were then integrated over the same duration. The net cavitation emissions from microbubbles could then be determined by subtracting the baseline measured prior to bubble administration.

It should be noted that the ultraharmonic responses may not be detected due to the high level of broadband noise, the ambient pressure (Sun *et al* 2012) and/or the presence of the skull. In order to ensure that the ultraharmonic signal can be distinguished from the variation of the background noise, i.e. to increase the signal-to-noise ratio (SNR), the following algorithm was used in the quantification. We first calculated the mean plus three times of the standard deviation of the signals in each in-harmonic range that was used in the ICD quantification. The calculated value was subsequently defined as the *noise level* of each ultraharmonic frequency bin prior to this in-harmonic range. The ultraharmonic cavitation event was considered observed only if the ultraharmonic value increased above the aforementioned noise level.

2.5. Acoustic parameters

2.5.1. Main study. In the main study, we chose 0.30–0.60 MPa FUS with microbubbles with three different size distributions to induce BBB opening based on previous reports using the same FUS experimental setup (Tung *et al* 2011b).

2.5.2. ICD-based safety assessments. A previous study (Chen and Konofagou 2014) indicated that delivering large compounds (>500 kDa) would be associated with the detection of strong inertial cavitation. In order to test the ICD-based safety assessments, we added two more groups with higher-pressure exposures (0.75 and 0.90 MPa) using 4–5 μm microbubbles to induce more inertial cavitation events.

2.6. MRI

All MR scans were performed using a 9.4 T MR system (DRX400, Bruker Medical, Billerica, MA). After each sonication and allowing 15 min for animal transport, each mouse was placed inside the vertical bore, while being anesthetized at 30–40 breaths min^{-1} with isoflurane gas (1%–2%). Pre-contrast T2 weighted, Dynamic contrast-enhanced MRI (DCE-MRI) and T1-weighted MR sequences were acquired on Day 0 and every 24 h up to 6 d. T2-weighted MRI was performed to detect edema using T2-RARE sequence (TR/TE: 3300/10.9 ms, spatial resolution: 86 × 86 μm^2, slice thickness: 500 μm). DCE-MRI was performed using a 2D FLASH T1-weighted sequence (TR/TE = 230/2.9 ms, spatial resolution: 130 × 130 μm^2, slice thickness: 600 μm). During the third acquisition of the dynamic sequence, the animal was injected with a 0.30 mL bolus of gadodiamide (Omniscan, GE Healthcare, Princeton, NJ) intraperitoneally (IP) as described elsewhere (Vlachos *et al* 2010). A T1-weighted 2D FLASH acquisition sequence (TR/TE: 230/3.3 ms, spatial resolution: 100 × 100 μm^2, slice thickness: 400 μm) was acquired 40 min after IP administration of gadodiamide.

The volume of opening/edema and permeability were analyzed following the approaches reported by our group (Samiotaki *et al* 2012, Samiotaki and Konofagou 2013, Wang *et al* 2014a). Briefly, the volume of opening was quantified with volumetric measurements of hyper-intense voxels in post-contrast T1-weighted MR images. Similarly, edema volume was calculated based on hyper-intense voxels in pre-contrast T2-weighted MR images. The permeability was assessed using the general kinetic model (GKM) on the basis of DCE-MR images (Vlachos *et al* 2010). The arterial input function in GKM was determined by averaging the gadodiamide concentration changes in the internal carotid artery from the entire cohort of wild-type mice. K_{trans}, the tracer transfer rate from blood plasma to extracellular extravascular space, served as the quantitative indicator of permeability.

2.7. Histology

All mice were euthanized and transcardially perfused with 30 mL PBS followed by 60 mL 4% paraformaldehyde on Day 7. The heads were harvested and then soaked in paraformaldehyde for 24 h, followed by skull removal and fixation again in 4% paraformaldehyde for 6 d. The brains were paraffin embedded and sectioned at 6 μm in thickness. Hematoxylin and eosin (H&E) staining was performed for histological analysis. For each brain, there were 32 sections prepared, with 180 μm spacing between planes.

2.8. Statistical analysis

An unpaired two-tailed Student's *t*-test was performed to compare the permeability coefficients between the treated and the sham group on each day. The cavitation dependence on the likelihood of no opening, safe opening or opening with damage was examined using one-way ANOVA, followed by a *post-hoc* Tukey's honest significant difference test. Error bars in this study represent standard deviations and values of $P < 0.05$ were considered significant. The

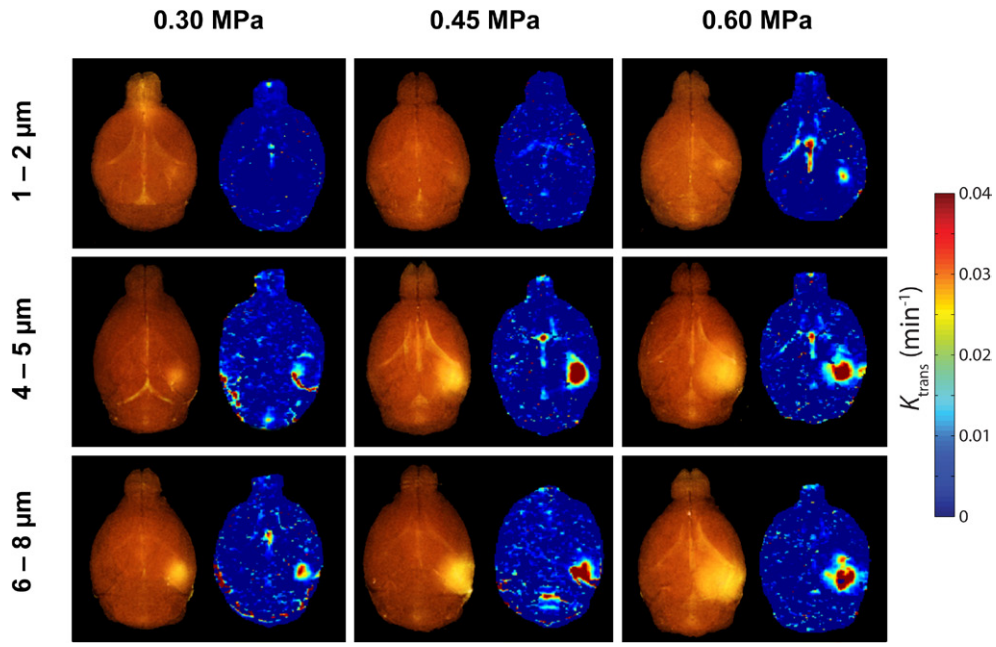

Figure 1. BBB opening evaluation. Typical 3D reconstructed T1-weighted MR images (shown in left for each group) and K_{trans} maps (shown in right for each group) of the central slice. The BBB opening assessments were microbubble-size and acoustic pressure dependent.

BBB was considered 'closed' when the opening volume fell below mean + three times of standard deviations of the sham group for each day. All statistical analyses were performed using GraphPad Prism 6 (La Jolla, CA).

3. Results

3.1. BBB opening

The opening volume and permeability of the BBB were assessed using MRI, as shown in figure 1. 3D T1-weighted MRI confirmed the opening and the corresponding K_{trans} maps provided the pharmacokinetic evaluations of different ultrasound parameters.

BBB opening were induced by 0.30–0.60 MPa FUS with monodispersed microbubbles within three different diameter ranges (table 1). As shown in figure 1 and table 1, opening volumes and K_{trans} coefficients were augmented as the FUS pressure and microbubble size increased. The bubble size effects were evident (table 1). Three opening outcomes listed in table 1 using 1–2 μm microbubbles were found to be dramatically different from those of larger bubbles. Interestingly, the opening can be reinstated within a specific BBB opening duration in the groups of '0.60 MPa, 1–2 μm' and '0.30 MPa, 4–5 μm' without any significant inter-animal variability, i.e. openings in Group '0.60 MPa, 1–2 μm' all closed on Day 1 and openings in Group '0.30 MPa, 4–5 μm' all closed on Day 3. It indicated that these two parameter sets could potentially be used to control the BBB recovery time reliably.

Table 1. Quantified opening volumes, K_{trans} coefficients and duration of BBB opening.

	Pressure											
	0.30 MPa				0.45 MPa				0.60 MPa			
Bubble diameter (μm)	n	Opening volume (mm^3)	K_{trans} (min^{-1})	Duration of opening (Day#)	n	Opening volume (mm^3)	K_{trans} (min^{-1})	Duration of opening (Day#)	n	Opening volume (mm^3)	K_{trans} (min^{-1})	Duration of opening (Day#)
1–2 μm	5	1.36 ± 2.72	0.004 ± 0.010	0.2 ± 0.40	4	1.67 ± 1.74	0.006 ± 0.002	0.6 ± 0.49	5	5.67 ± 3.75	0.011 ± 0.006	1.0 ± 0
4–5 μm	4	11.12 ± 0.73	0.012 ± 0.002	3.0 ± 0	7	31.10 ± 5.37	0.020 ± 0.004	4.8 ± 0.40	5	45.33 ± 3.22	0.026 ± 0.006	4.4 ± 0.49
6–8 μm	5	15.36 ± 2.61	0.016 ± 0.007	3.2 ± 0.75	6	35.42 ± 4.62	0.025 ± 0.004	3.8 ± 0.75	5	44.65 ± 8.90	0.031 ± 0.005	4.7 ± 0.47

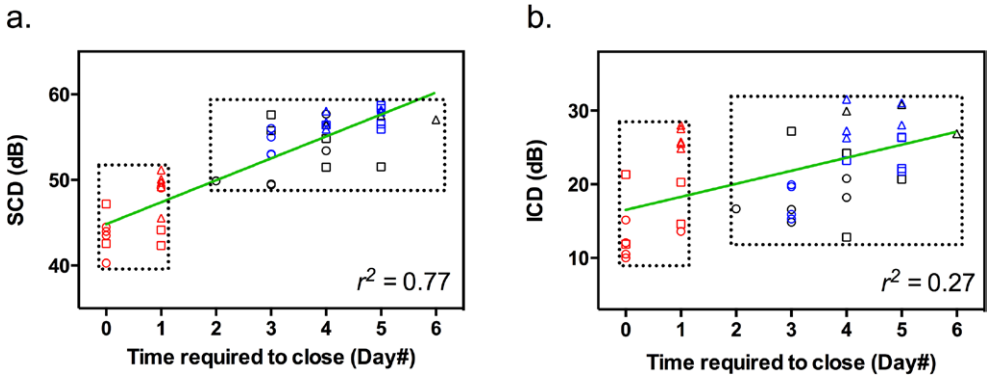

Figure 2. Measured (a) stable and (b) inertial cavitation doses on the sonication day as a function of the duration of BBB opening. Number of mice: 41 (excluding the cases with LO, the sham group and one off-target case); 1–2, 4–5 and 6–8 μm groups were labeled in red, blue and black, respectively; 0.30, 0.45 and 0.60 MPa groups were marked by circle, square and upper triangle, respectively.

3.2. Cavitation dependence of time required to close

To investigate whether the cavitation dose can be a promising indicator to predict the reversibility of BBB, the temporal variation of SCD and ICD was obtained (figure 2). The SCD showed good agreement ($r^2 = 0.77$) with closing time, suggesting that the SCD could potentially be used in predicting reversibility. However, the ICD-based prediction was not shown as reliable ($r^2 = 0.27$). In addition, the duration of the opened BBB was found to be bubble-size dependent (figure 2). Smaller microbubbles (1–2 μm) induced shorter openings within 1 d, while larger bubbles (4–5 and 6–8 μm) produced longer openings up to 2–6 d. Consistent with the bubble-size effects in the opening assessments, stable cavitation activities of 1–2 μm microbubbles can be differentiated from those of larger bubbles ($P < 0.0001$) with a threshold level at around 50 dB (figure 2(a)). The ICD of 1–2 μm microbubbles were also found to be statistically different (figure 2(b); $P < 0.05$) compared to that of larger bubbles.

3.3. Permeability and its cavitation relevance

The permeability closing timeline was characterized both qualitatively and quantitatively in figure 3. Four mice were found to have 6 d-long openings based on T1-weighted MRI assessment on Day 6. We define those four animals as *Long-term Opening* (LO) cases, while others that closed within Day 1–6 are *Reversible Opening* (RO) cases. LO cases showed higher permeability coefficients than that of RO cases for each day of the experiment. In addition, K_{trans} of LO was found to be significantly higher compared to that of the sham till Day 4. However, the K_{trans} of the RO decreased to the same level as that of sham after Day 1, indicating that the 'open' state of LO lasted longer than that of RO. Interestingly, the K_{trans} closing curves of RO and LO (figure 3) underwent different temporal variations. K_{trans} in the LO cases reached a peak on Day 1 and then gradually declined while K_{trans} in the RO cases decreased monotonically.

Having established the relationship between cavitation responses and reversibility of the opened BBB, we further investigated the relationship between cavitation dose and permeability coefficient. Both SCD ($r^2 = 0.82$) and ICD ($r^2 = 0.73$) were found to be linearly correlated

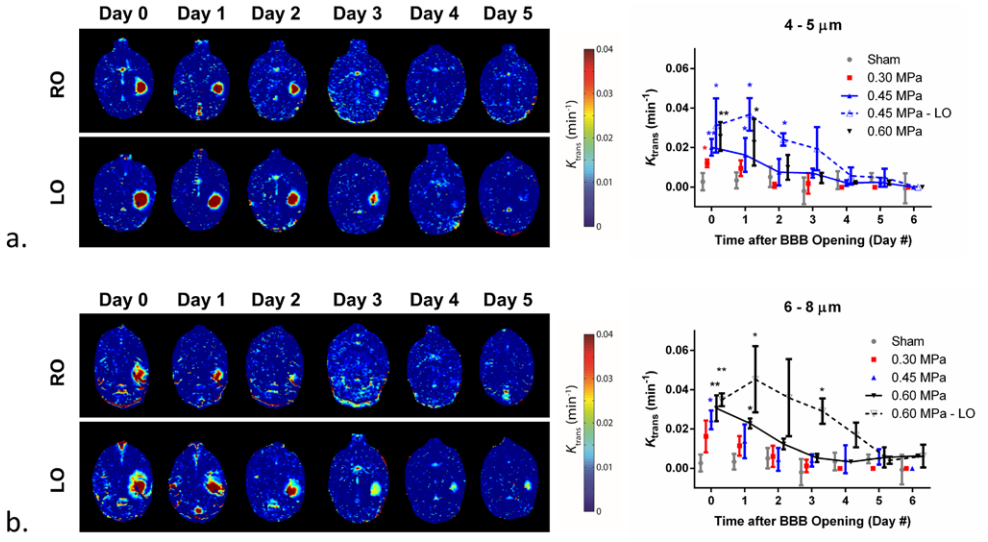

Figure 3. Permeability (K_{trans}) closing timeline. Typical permeability maps and K_{trans} measured of (a) 4–5 μm and (b) 6–8 μm groups. Number of mice: 48 (excluding one off-target case); Sham, 0.30, 0.45 and 0.60 MPa groups were labeled in grey, red, blue and black, respectively; RO: reversible opening; LO: long-term opening. All statistical analyses were *t*-tests compared with the sham group for each day. *: $P < .05$; **: $P < .01$. Error bar represents mean ± standard deviation std.

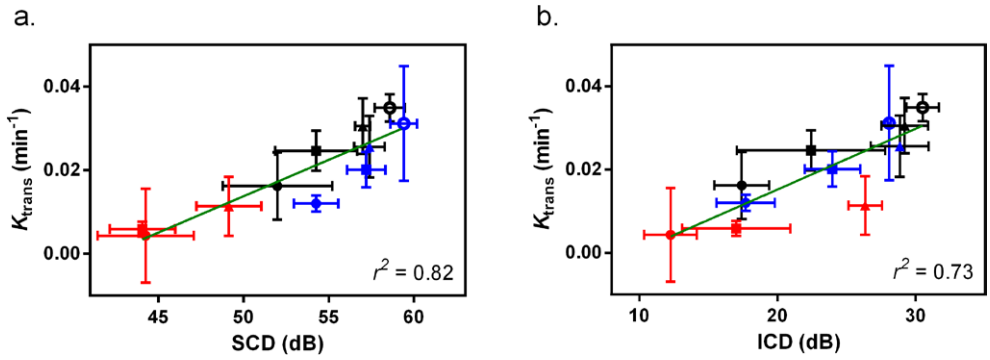

Figure 4. (a) Stable and (b) inertial cavitation dose dependencies on the permeability coefficients on the sonication day. Number of mice: 45 (excluding the sham group and one off-target case); 1–2, 4–5 and 6–8 μm groups were labeled in red, blue and black, respectively; 0.30, 0.45 and 0.60 MPa groups were marked by circle, square and upper triangle, respectively. LO subjects were labeled in hollow circles. Error bar represents mean ± std.

with the K_{trans} on the sonication day (figure 4). K_{trans} of LO cases and their corresponding SCDs held the largest values among others.

3.4. Safety analysis

To identify edema and neurovascular damage after ultrasound exposure, we performed pre-contrast T2-weighted MRI and H&E histological analyses, respectively. Damage, including

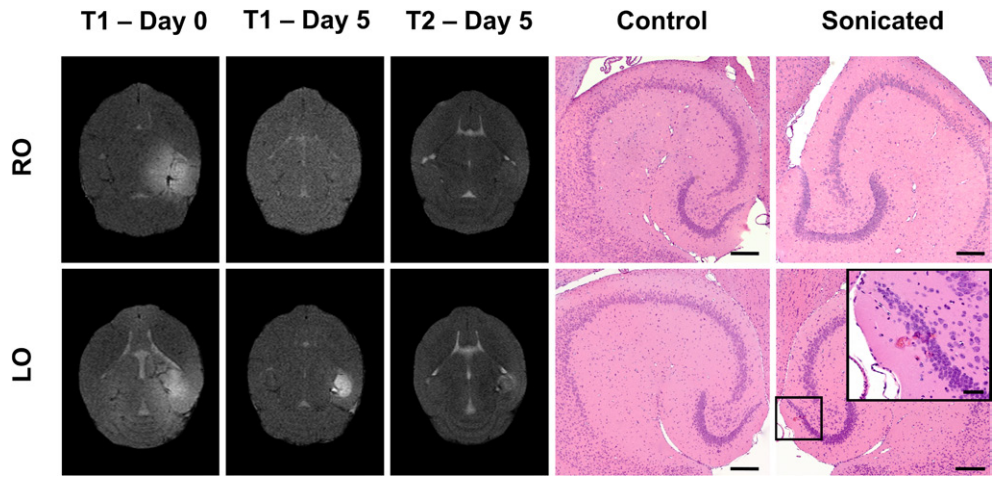

Figure 5. Safety assessments. T1-w on Day 0, T1-w and T2-w MR images on Day 5, Histologic evaluation (H&E) of the control and sonicated sides were compared between RO and LO cases under the same ultrasound parameters (0.60 MPa, 6–8 μm microbubbles). Scale bars = 200 μm; scale bar in the inset = 50 μm.

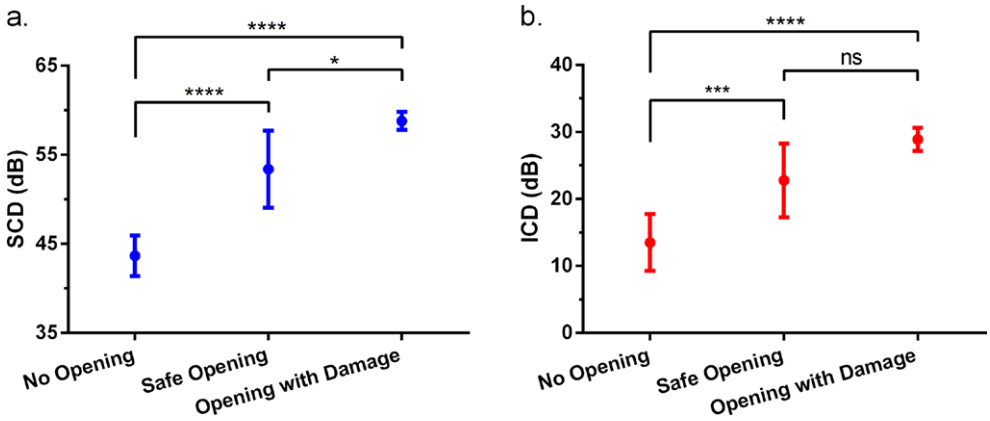

Figure 6. Measured (a) stable and (b) inertial cavitation doses compared across no opening, safe opening and opening with damage cases. Number of mice: 46 (excluding the sham group); *: $P < .05$; ***: $P < .001$; ****: $P < .0001$; ns: no significance. Error bar represents mean $\pm$ std.

red blood cell extravasations and dark neurons, was found in four mice (excluding the one under off-targeting exposure), which were also the four LO cases. Figure 5 compared the opening volumes, T2 enhancements and H&E staining results of the RO and LO cases under the same FUS exposure. Contrary to the RO subjects, the BBB of the LO subjects remained open with edema on Day 5.

All animals in the main study excluding the sham group were then categorized into three groups according to the H&E evaluations (figure 6). Cavitation responses among the three groups were compared using one-way ANOVA. The ANOVA showed significance and the *post-hoc* multi-comparison revealed the significantly different SCD ($P < 0.05$) compared

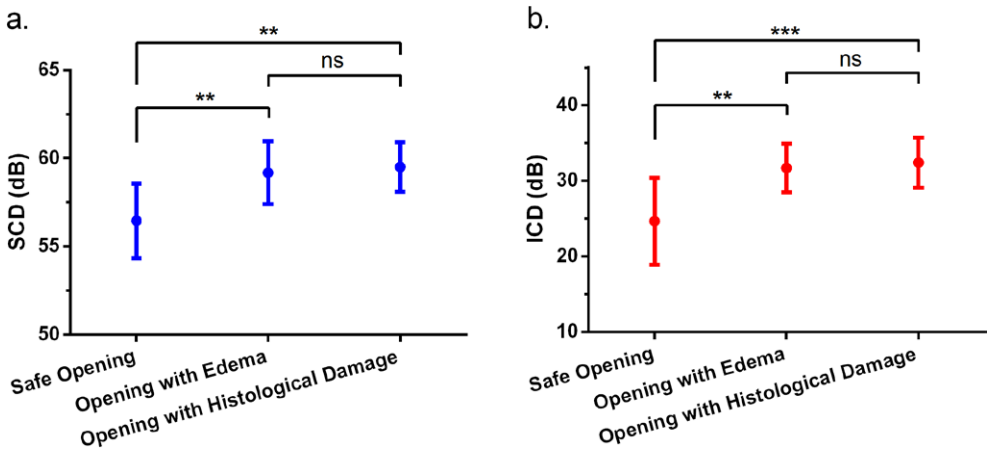

Figure 7. Measured (a) stable and (b) inertial cavitation doses compared across safe opening, opening with edema and opening with histological damage cases. Number of mice: 29 (4–5 μm microbubbles, pressures: 0.30, 0.45, 0.60, 0.75 and 0.90 MPa); **: $P < .01$; ***: $P < .001$; ns: no significance. Error bar represents mean $\pm$ std.

across 'no opening', 'safe opening' and 'opening with damage' cases. Note that the four cases with histological damage are the same cases with edema on Day 5 so that we did not differentiate the edema and histological damage. These findings indicate that the SCD may also be used as a measure of likelihood for safe opening, which further demonstrated the reliability of SCD-based prediction of opening outcomes.

Finally, in order to further investigate the ICD-based prediction of the safety assessments, we did an extensive study including two more groups with higher-pressure exposures (0.75 and 0.90 MPa) using 4–5 μm microbubbles. Figure 7 showed the cavitation comparisons across 'safe openings', 'opening with edema' and 'opening with histological damage' (Note that all the subjects were successfully opened by 0.30–0.90 MPa FUS with 4–5 μm microbubbles). These results revealed the significantly different SCD ($P < 0.01$) and ICD ($P < 0.01$) compared across safe opening, opening with edema and opening with histological damage subjects. The ICD-based prediction of safety could thus be accomplished after FUS exceeds certain pressure (i.e. stronger inertial cavitation activities are induced).

4. Discussion

In this study, the feasibility of assessing the restoration and pharmacokinetics of FUS-opened BBB based on monitoring cavitation signals was investigated. Our results revealed that stable cavitation signals from oscillating microbubbles can be utilized to potentially predict and control the duration of BBB opening, the likelihood of safe opening and the permeability of the opened BBB. A real-time feedback method based on monitoring SCD could then be used to control and predict the physiological changes during FUS exposure.

4.1. Cavitation dependence and mechanisms

Our results indicated that, at low to moderate pressure levels (0.30–0.60 MPa) *in vivo*, SCD showed good correlations with the reinstatement time, likelihood of safe opening and K_{trans};

while ICD was only well correlated with K_{trans}. Possible causes may be attributed to cavitational mechanisms. Sustained stable cavitation could thus be the dominant physical mechanism in opening the BBB at low to moderate pressure levels, at which FUS exposures are normally kept to avoid damage to the brain. The inertial cavitation threshold is higher than the occurrence of sustained stable cavitation (Bader and Holland 2013). Within the range of 0.30–0.60 MPa, stable cavitating microbubbles cause physiological effects, while only a small number of nuclei undergo inertial cavitation (Tung *et al* 2011b). Stable cavitation may thus dominate the cavitation activities to induce BBB opening.

Additionally, SCD may also be used to gauge the likelihood for safe opening. This finding is in agreement with the numerical investigation by Bader *et al* (Bader and Holland 2013). The threshold of inertial cavitation predicted by the Mechanical Index (MI, PRP / $\sqrt{f_c}$), which is the standard indicator for adverse bio-effects, is MI = 0.4 (Holland *et al* 2000, Bader and Holland 2013). The cavitation index (I_{CAV}, PRP / f_c) was developed by Bader *et al* to predict the occurrence of stable cavitation. Stable cavitation components are likely to occur when $0.09 \leqslant I_{CAV} \leqslant 0.45$ (Bader and Holland 2013). The parameters used in the present study (0.30–0.60 MPa at 1.5 MHz) appeared in the range of I_{CAV} from 0.2 to 0.4, and MI from 0.245 to 0.49, suggesting that the likelihood of stable cavitation was evident and that of the inertial cavitation was lower (i.e. smaller number of nuclei would undergo inertial cavitation).

4.2. Pharmacodynamic evaluations

The good correlation between cavitation responses with BBB permeability (figure 4) indicated that monitoring cavitation activities would aid in monitoring the pharmacokinetics of the drugs to be delivered. Interestingly, figure 3 showed that the K_{trans} peak in the LO cases was reached 24 h after BBB opening, whereas the permeability of RO decreased as time progressed. This may be attributed to the edema that was detected until Day 5 (figure 5). T2-weighted MR images of LO subjects indicated larger hyper-intense areas on the sonicated side on Day 1 than that on Day 0. The existence of edema may affect the contrast in DCE-MRI as well as the quantification of K_{trans}.

4.3. Control the opening

To monitor and control the opening using real-time feedback during FUS is the ultimate goal for clinical translation. O'Reilly *et al* (O'Reilly and Hynynen 2012) designed a semi-closed-loop controlling system for BBB opening. They detected ultraharmonic components in the loop, and decreased the pressure to different target levels (% pressure to achieve ultraharmonics) once ultraharmonic emission detected. Target levels were found to be associated with MRI enhancement and damage occurrence. Albeit the potential of this controlling paradigm, one limitation is that the controlling relied on the successful detection of ultraharmonics, and then it became open-loop for the remainder of the sonications. However, it has been reported that ultraharmonic emissions were only occasionally observed in some PCD systems (Arvanitis *et al* 2012), which might affect the performance of ultraharmonic-based controller. Moreover, many other important matrixes, such as the cavitation doses of harmonics and broadband noise, had not been implemented into the feed-back control. Based on our findings, monitoring of these cavitation doses is associated with not only the direct opening assessments (such as MRI and/or fluorescence contrast enhancement), but also the other opening's characteristics (such as the opening duration, safety and permeability). To achieve the desired opening, FUS pressure, PL and/or PRF can be programmed based on the cavitation monitoring feedback. In addition, the cumulative cavitation doses may serve as the end or critical turning point

of FUS exposure. For example, one can stop or decrease the level of FUS exposure once a certain amount of SCD and/or ICD has been reached. However, it should be noted that results of the present study were in agreement with O'Reilly *et al*'s that the damage occurrence did not correlate with wideband responses well while it was associated with strong stable cavitation response. It suggested that the window to achieve safe opening was limited and we may have to be conservative in setting the parameters in the controller. For instance, one may want to avoid opening in 5 days due to the safety concern.

Prior to FUS exposure, selecting more suitable parameter sets also becomes important in tailoring the opening. In this study, cavitation activities were induced by microbubbles in FUS fields with various acoustic pressures. In order to reliably tailor the opening, we have uncovered the optimal type of bubble and FUS pulse trains. For instance, the BBB can be reinstated with 100% probability within the same amount of time when sonicated under the following parameter sets: [0.60 MPa, 1–2 μm] (closed on Day 1) and [0.30 MPa, 4–5 μm] (closed on Day 3). These two parameter sets may be used to control the BBB reversibility more reliably than other parameter sets.

4.4. Safety assessments

Typically attributed to adverse bio-effects, inertial cavitation is normally intended to be avoided by lowering FUS pressure in opening the BBB (Tung *et al* 2011b) and other microbubble-mediated ultrasound therapy (Bader and Holland 2013). We have demonstrated that SCD can serve as a reliable indicator to gauge the likelihood for safe opening at a low to medium pressure range. However, previous reports (Chen and Konofagou 2014) have shown that inertial cavitation has been associated with the successful delivery of agents larger than 500 kDa when Definity® is used. This finding suggests that delivering larger-size agents may require inertial cavitation when smaller bubbles are used. Our results (figure 7) indicated that ICD-based safety control could be accomplished when stronger inertial cavitation activities are induced, which would ultimately help clinicians to monitor the likelihood of safe opening during treatment using ICD.

Another interesting finding is that the cases with 'opening with edema' and cases with 'opening with histological damage' were identical under 0.60 MPa, while they did not fully coincide at 0.75 and 0.90 MPa. Three different situations were then found: (1) with edema but without histological damage; (2) without edema but with histological damage; and (3) with edema and with histological damage. The first situation can be attributed to the sensitivity of H&E histological evaluations. The second may result from physiological reinstatement of BBB. Future studies will investigate the detailed physiological mechanisms and their correlation with cavitation activities.

4.5. Limitations

There are several limitations to this study. First, MRI assessment was performed on a daily basis, so that the detection of closing is not precise in terms of hours. In other words, the time required for BBB reinstatement may be overestimated by no more than 24 h. Moreover, it should be noted that the opening findings are tied to the MR tracer used in the assessments. Based on our previous results assessed by fluorescently tagged dextrans, the position and areas of opening were agent-size relevant (Choi *et al* 2010). Thus, MR contrast agents at different molecular weights would result in distinct reversibility and permeability outcomes. Lastly, the global cavitation matrixes (SCD and ICD) were found to be bubble-size dependent. It would be interesting to normalize the SCD and ICD by an appropriate scaling factor, such as the scattering cross section of microbubbles, so that more detailed cavitation mechanisms may

be uncovered. The cross section of larger bubbles would result in more scattering, and thus more cavitation emissions (Ainslie and Leighton 2011). Unfortunately, it is hard to calculate the scattering cross section at this time, since an elaborate simulation study will need to be performed. We will assess this effect in our future work.

5. Conclusion

In summary, we have shown that monitoring of the cavitation behavior during FUS can reliably predict the duration of opening, the permeability of the induced BBB opening and the likelihood of safe opening. The stable cavitation dose may therefore provide a real-time predictor of the properties of the induced reversible disruption. Finally, the dependence of the BBB reversibility on the bubble diameter and FUS pressure allows for the control of the safety profile of this technique.

Acknowledgments

This study was supported in part by National Institute of Health grants R01 EB009041 and R01 AG038961. The authors wish to thank Dr Yao-Sheng Tung, Oluyemi Olumolade, Anushree Srivastava, Dr Hong Chen, Shih-Ying Wu, and Dr Fabrice Marquet from Biomedical Engineering Department of Columbia University, for their important assistance and suggestions.

Reference

Ainslie M A and Leighton T G 2011 Review of theory for scattering and extinction cross-sections, damping factors and resonance frequencies of spherical gas bubbles *J. Acoust. Soc. Am.* **130** 3184–208

Arvanitis C D, Livingstone M S and McDannold N 2013 Combined ultrasound and MR imaging to guide focused ultrasound therapies in the brain *Phys. Med. Biol.* **58** 4749–61

Arvanitis C D, Livingstone M S, Vykhodtseva N and McDannold N 2012 Controlled ultrasound-induced blood-brain barrier disruption using passive acoustic emissions monitoring *PLoS One* **7** e45783

Aryal M, Arvanitis C D, Alexander P M and McDannold N 2014 Ultrasound-mediated blood-brain barrier disruption for targeted drug delivery in the central nervous system *Adv. Drug Deliv. Rev.* **72** 94–109

Bader K B and Holland C K 2013 Gauging the likelihood of stable cavitation from ultrasound contrast agents *Phys. Med. Biol.* **58** 127–44

Burgess A and Hynynen K 2013 Noninvasive and targeted drug delivery to the brain using focused ultrasound *ACS Chem. Neurosci.* **4** 519–26

Chen H, Chen C C, Acosta C, Wu S-Y, Sun T and Konofagou E E 2014 A new brain drug delivery strategy: focused ultrasound-enhanced intranasal drug delivery *PLoS One* **9** e108880

Chen H and Konofagou E E 2014 The size of blood-brain barrier opening induced by focused ultrasound is dictated by the acoustic pressure *J. Cereb. Blood Flow Metab.* **34** 1197–204

Choi J J, Pernot M, Small S A and Konofagou E E 2007 Noninvasive, transcranial and localized opening of the blood-brain barrier using focused ultrasound in mice *Ultrasound Med. Biol.* **33** 95–104

Choi J J, Wang S, Tung Y-S, Morrison B and Konofagou E E 2010 Molecules of various pharmacologically-relevant sizes can cross the ultrasound-induced blood-brain barrier opening *in vivo Ultrasound Med. Biol.* **36** 58–67

Fan C-H, Liu H-L, Ting C-Y, Lee Y-H, Huang C-Y, Ma Y-J, Wei K-C, Yen T-C and Yeh C-K 2014 Submicron-bubble-enhanced focused ultrasound for blood-brain barrier disruption and improved CNS drug delivery *PLoS One* **9** e96327

Ferrara K, Pollard R and Borden M 2007 Ultrasound microbubble contrast agents: fundamentals and application to gene and drug delivery. *Annu. Rev. Biomed. Eng.* **9** 415–47

Feshitan J A, Chen C C, Kwan J J and Borden M A 2009 Microbubble size isolation by differential centrifugation *J. Colloid Interface Sci.* **329** 316–24

Holland C K, O'Brien W D Jr, Crum L A, Ferrer P L and Tarantal A F 2000 Bioeffects in tissues with gas bodies *J. Ultrasound Med.* **19** 97–108 (www.jultrasoundmed.org/content/19/2/97.abstract)

Hsu P-H, Wei K-C, Huang C-Y, Wen C-J, Yen T-C, Liu C-L, Lin Y-T, Chen J-C, Shen C-R and Liu H-L 2013 Noninvasive and targeted gene delivery into the brain using microbubble-facilitated focused ultrasound *PLoS One* **8** e57682

Hynynen K and McDannold N 2001 Noninvasive MR imaging–guided focal opening of the blood-brain barrier in rabbits *Radiology* **220** 640–6

Kinoshita M, McDannold N, Jolesz F A and Hynynen K 2006 Targeted delivery of antibodies through the blood-brain barrier by MRI-guidedl focused ultrasound *Biochem. Biophys. Res. Commun.* **340** 1085–90

Liu H-L, Hua M-Y, Chen P-Y, Chu P-C, Pan C-H, Yang H-W, Huang C-Y, Wang J-J, Yen T-C and Wei K-C 2010 Blood-brain barrier disruption with focused ultrasound enhances delivery of chemotherapeutic drugs for glioblastoma treatment *Radiology* **255** 415–25

McDannold N, Arvanitis C D, Vykhodtseva N and Livingstone M S 2012 Temporary disruption of the blood-brain barrier by use of ultrasound and microbubbles: safety and efficacy evaluation in rhesus macaques *Cancer Res.* **72** 3652–63

McDannold N, Vykhodtseva N and Hynynen K 2006 Targeted disruption of the blood-brain barrier with focused ultrasound: association with cavitation activity *Phys. Med. Biol.* **51** 793–807

O'Reilly M and Hynynen K 2012 Blood-brain barrier: real-time feedback-controlled focused ultrasound disruption by using an acoustic emissions–based controller *Radiology* **263** 96–106

Pardridge W M 2005 The blood-brain barrier: bottleneck in brain drug development. *NeuroRx* **2** 3–14

Park J, Zhang Y, Vykhodtseva N, Jolesz F A and McDannold N J 2012 The kinetics of blood brain barrier permeability and targeted doxorubicin delivery into brain induced by focused ultrasound *J. Control. Release* **162** 134–42

Qin S, Caskey C F and Ferrara K W 2009 Ultrasound contrast microbubbles in imaging and therapy: physical principles and engineering *Phys. Med. Biol.* **54** R27–57

Raymond S B, Treat L H, Dewey J D, McDannold N J, Hynynen K and Bacskai B J 2008 Ultrasound enhanced delivery of molecular imaging and therapeutic agents in Alzheimer's disease mouse models *PLoS One* **3** e2175

Samiotaki G, Acosta C, Wang S and Konofagou E E 2015 Enhanced delivery and bioactivity of the neurturin neurotrophic factor through focused ultrasound—mediated blood–brain barrier opening *in vivo J. Cereb. Blood Flow Metab.* **35** 611–22

Samiotaki G and Konofagou E 2013 Dependence of the reversibility of focused-ultrasound-induced blood–brain barrier opening on pressure and pulse length *in vivo IEEE Trans. Ultrason.* **60** 2257–65

Samiotaki G, Vlachos F, Tung Y-S and Konofagou E E 2012 A quantitative pressure and microbubble-size dependence study of focused ultrasound-induced blood-brain barrier opening reversibility *in vivo* using MRI *Magn. Reson. Med.* **67** 769–77

Sun T, Jia N, Zhang D and Xu D 2012 Ambient pressure dependence of the ultra-harmonic response from contrast microbubbles *J. Acoust. Soc. Am.* **131** 4358–64

Thévenot E, Jordão J F, O'Reilly M A, Markham K, Weng Y-Q, Foust K D, Kaspar B K, Hynynen K and Aubert I 2012 Targeted delivery of self-complementary adeno-associated virus serotype 9 to the brain, using magnetic resonance imaging-guided focused ultrasound. *Hum. Gene Ther.* **23** 1144–55

Treat L H, McDannold N, Zhang Y, Vykhodtseva N and Hynynen K 2012 Improved anti-tumor effect of liposomal doxorubicin after targeted blood-brain barrier disruption by MRI-guided focused ultrasound in rat glioma *Ultrasound Med. Biol.* **38** 1716–25

Tung Y-S, Marquet F, Teichert T, Ferrera V and Konofagou E E 2011a Feasibility of noninvasive cavitation-guided blood-brain barrier opening using focused ultrasound and microbubbles in nonhuman primates *Appl. Phys. Lett.* **98** 163704

Tung Y-S, Vlachos F, Choi J J, Deffieux T, Selert K and Konofagou E E 2010 *In vivo* transcranial cavitation threshold detection during ultrasound-induced blood-brain barrier opening in mice *Phys. Med. Biol.* **55** 6141–55

Tung Y-S, Vlachos F, Feshitan J A, Borden M A and Konofagou E E 2011b The mechanism of interaction between focused ultrasound and microbubbles in blood-brain barrier opening in mice *J. Acoust. Soc. Am.* **130** 3059–67

Vlachos F, Tung Y-S and Konofagou E 2011 Permeability dependence study of the focused ultrasound-induced blood-brain barrier opening at distinct pressures and microbubble diameters using DCE-MRI *Magn. Reson. Med.* **66** 821–30

Vlachos F, Tung Y-S and Konofagou E E 2010 Permeability assessment of the focused ultrasound-induced blood-brain barrier opening using dynamic contrast-enhanced MRI *Phys. Med. Biol.* **55** 5451–66

Wang F *et al* 2012 Targeted delivery of GDNF through the blood-brain barrier by MRI-guided focused ultrasound *PLoS One* **7** e52925

Wang S, Olumolade O O, Sun T, Samiotaki G and Konofagou E E 2015 Noninvasive, neuron-specific gene therapy can be facilitated by focused ultrasound and recombinant adeno-associated virus *Gene Ther.* **22** 104–10

Wang S, Samiotaki G, Olumolade O, Feshitan J A and Konofagou E E 2014a Microbubble type and distribution dependence of focused ultrasound-induced blood-brain barrier opening *Ultrasound Med. Biol.* **40** 130–7

Wang S, Sun T, Acosta C, Karakatsani M E, Olumolade O and Samiotaki G 2014b Enhancement of direct brain infusion with focused ultrasound and microbubbles *2014 IEEE Int. Ultrasonics Symp. Proc.* pp 2169–72